Baseline study for higher moments of net–charge multiplicity distribution at RHIC energies

Nihar R. Sahoo, Sudipan De and Tapan Nayak
Variable energy cyclotron center, Kolkata - 700064, India

Lattice QCD models predict the presence of a critical point in the QCD phase diagram where the first order phase transition between the hadron gas and Quark-Gluon Plasma ceases to exist. Higher moments of conserved quantities, such as net–charge, net–baryon number and net–strangeness, and their products, are proposed as sensitive probes for locating the critical point. The higher moments of net–charge multiplicity distributions have been studied for RHIC energies for Au-Au collisions at $\sqrt{s_{\rm NN}} = 7.7$ to 200 GeV using three event generators, *viz.*, HIJING, UrQMD and THERMINATOR-2. We discuss the effects of centrality selection, resonance production, as well as different particle species on the net–charge moments and their products. Finally, we present the model predictions on higher moments which set the baseline for measurements at RHIC.

PACS numbers: 25.75.-q

I. INTRODUCTION

The Relativistic Heavy-Ion Collider (RHIC) at Brookhaven National Laboratory is a dedicated facility for the search and study of Quark-Gluon Plasma (QGP) and to explore the QCD (Quantum Chromodynamics) phase transition. The phase diagram, plotted in terms of baryon chemical potential (μ_B) and temperature (T) depicts the transition from QGP to a state of matter consisting of hadron gas (HG). Lattice QCD based models reveal that at vanishing μ_B, the transition from QGP to HG is a simple crossover [1], whereas at large μ_B, the phase transition is of first order [1–7]. Thus a critical point in the QCD phase diagram is expected at the point where the first order transition ends. In recent years, probing the location of the critical point has been one of the primary goals of the physics program at RHIC. The QCD phase diagram is scanned by varying the center-of-mass energy of heavy-ion collisions at RHIC, thereby changing the μ_B and T in a controlled manner. It has been predicted that the location of the critical point could be signaled by the non-monotonic behavior in several fluctuation observables as a function of the beam energy.

Lattice and other QCD based models predict that higher moments of conserved quantities, such as net–charge, net–baryon number, net–strangeness, and net–isospin distributions, provide the most sensitive probes of the critical point. This is because of the fact that at the critical point, thermodynamic susceptibilities and the correlation length (ξ) of the system diverge [4, 7, 8]. The moments of the distributions, mean (M), standard deviation (σ), skewness (S) and kurtosis (κ), are related to the higher order thermodynamic susceptibilities of the conserved quantities and also to the correlation length. For example, the variance, skewness and kurtosis have been shown to be related to the ξ^2, $\xi^{4.5}$ and ξ^7, respectively [8]. In order to cancel the volume term in the susceptibilities, different combinations of the various moments are constructed, some of these are: M/σ^2, $S\sigma$ and $\kappa\sigma^2$. These products, as a function of beam energy, are expected to show non-monotonic behaviour near the critical point.

Experimental study of net–charge fluctuations may have some the advantages over other conserved quantities. Fluctuations of net–charges are related to the net–baryon and net–isospin fluctuations [9]. Due to the problem with detection of neutrons in heavy ion experiments, it has been shown that net–proton may not be a good proxy for the net–baryon [10, 11]. On the other-hand, the net–charge takes into account all charged particles produced in the heavy ion collisions. Other analytical calculation [12] suggests that the net–charge higher moment analysis may be less affected by effect of acceptance as compared to that of net–proton. Recent lattice QCD model estimations [13] add new motivation for higher moments analysis to extract the freeze-out parameter from the lattice QCD calculation.

To map the QCD phase diagram and to locate the critical point, the beam energy scan program [14–16] has started in the year 2010 at RHIC. The program aims to scan the beam energy from $\sqrt{s_{\rm NN}} = 7.7$ to 39 GeV including 62.4 and 200 GeV, corresponding to baryon chemical potentials from 450 MeV to 20 MeV [17].

In this study, the QCD based model (HIJING [18]), transport model (UrQMD [19]) and thermal model (THERMINATOR-2 [20]) are used to study fluctuations of net–charge. To understand the various physics processes, like jet and mini-jet production by HIJING, hadronic re-scattering and various resonance decay by UrQMD and thermal production of particles by THERMINATOR-2 are used as background for this analysis. The above models are blind to the critical phenomena in the heavy ion collision physics. Thus, these models help

to understand the baseline for the higher moments of the net–charge distributions.

Rest of the article is organized as follows. In the next section, we introduce the net–charge moments. In section III, we study the importance of centrality selection and show how centrality bin width correction can be used. In section IV, we discuss the contributions of different particle species on the net–charge moments. In section V, resonance effects are studied. Finally in section VI, we present the products of moments from different event generators and compare to that of the hadron gas model. We conclude with a summary and outlook for future studies in this direction.

II. MOMENTS OF NET–CHARGE DISTRIBUTIONS

In an experimental scenario, both the positive and negative charges are measured in a finite acceptance on an event-by-event basis. From these, the net–charge (difference between the positive and negative charges) distributions are obtained in a narrow window in centrality. These distributions are to be analyzed to obtain various moments. The first four moments are expressed as,

$$\begin{aligned} \text{Mean}: \quad & M =< N >, \\ \text{variance}: \quad & \sigma^2 =< (\delta N)^2 >, \\ \text{skewness}: \quad & S = \frac{< (\delta N)^3 >}{\sigma^3}, \text{ and} \\ \text{kurtosis}: \quad & \kappa = \frac{< (\delta N)^4 >}{\sigma^4} - 3, \end{aligned} \tag{1}$$

where $N = N_+ - N_-$ is the net charge and $\delta N = (N - < N >)$. The variance depicts the width of the distribution, the skewness is a measure of the asymmetry of the distribution, and kurtosis gives an indication of whether the distribution is picked at the center or not.

Net–charge multiplicity distributions are sensitive to centrality of the collision. Centrality is normally expressed in terms of impact parameter of the collision or by percentage of total cross sections (0-5% being most central) or by the number of participating nucleons ($N_{\rm part}$). Different centrality classes are defined within a narrow range of $N_{\rm part}$. The average value of $N_{\rm part}$ for different centrality class is estimated from Glauber model calculations.

The beam energy dependence of the net–charge distributions for central collisions has been studied using different models by choosing the charged and identified particles selected within pseudo-rapidity range of $|\eta| = 0.5$ and transverse momentum range, $0.2 < p_{\rm T} < 2.0$ GeV/c. In Fig. 1(a), this is shown for the UrQMD event generator, for four different center-of-mass energies. With the increase of beam energy, the total number of charged particle multiplicity increases and particle to anti-particle ratio tends to unity. Thus the mean of the distribution get closer to zero and the distribution gets wider for increasing center-of-mass energy.

Centrality dependence of the net–charge distributions can be studied by plotting the distributions for various centralities. Fig. 1(b) shows the net–charge distributions for three different centrality classes for Au-Au collisions at $\sqrt{s_{NN}} = 39$ GeV, obtained from the UrQMD model. It can be seen that the width of the net-charge distribution decreases as we go from central to peripheral events. Moreover, the mean of the distribution also shifts to higher values in going from central to peripheral events. The moments of the distributions are sensitive to the width of the centrality window, which needs to be dealt with properly. This will be discussed in the following section.

III. CENTRALITY BIN WIDTH EFFECT ON HIGHER MOMENTS

Moments of the distributions are obtained from net–charge distributions for a given centrality class. A given centrality class is a collection of different events having different impact parameters. Collision at the given impact parameter represents corresponding volume of the collision geometry. Due to event-by-event estimations, distributions corresponding to several different impact parameters contribute with a given centrality window. This results in additional fluctuations within each centrality class. Due to this effect, the value of the moments gets affected with increase in centrality bin width. This centrality bin width effect can be see in Fig. 2 where we plot the first four moments of net–charge distributions for Au-Au collisions at $\sqrt{s_{\rm NN}} = 39$ GeV. This is plotted for three centrality bin widths corresponding to 2.5%, 5%, and 10%. It shows first two moments, M and σ are not so much affected for different widths, but the S and κ's values are very much affected by these effect. The variation for larger bin width as a function of centrality is quite large. Due to this effect, these moments increase with increase in centrality bin width. This effect needs to be corrected for moments analysis. To correct this effect, the direct weighted method [21] is used. In this method instead of direct estimation of higher moments in a given centrality class, following weighted averages are used:

$$X = \frac{\sum_i n_i X_i}{\sum_i n_i}, \tag{2}$$

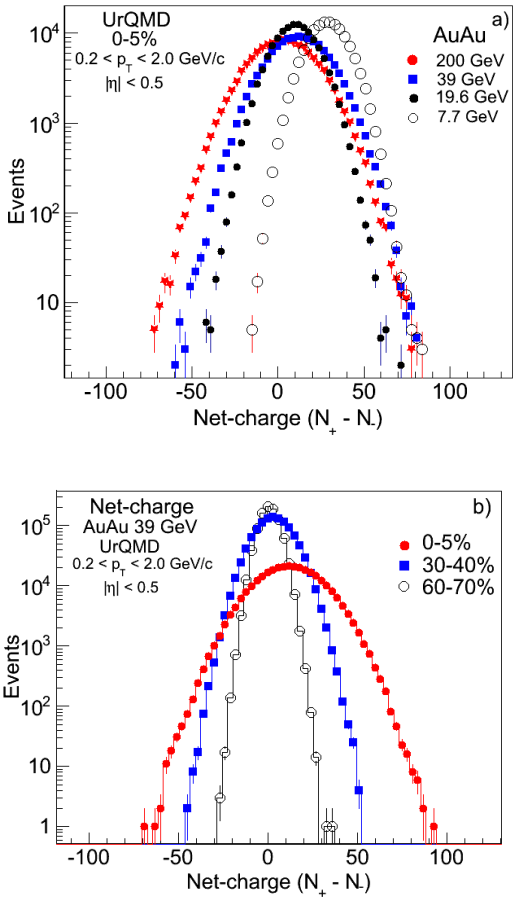

FIG. 1: The net–charge multiplicity distributions obtained from the UrQMD model for Au-Au collisions as a function of (a) centrality, expressed in terms of percentage or cross section for $\sqrt{s_{\rm NN}}$=39 GeV, and (b) collision energy for $\sqrt{s_{\rm NN}}$=7.7, 19.6, 39 and 200 GeV.

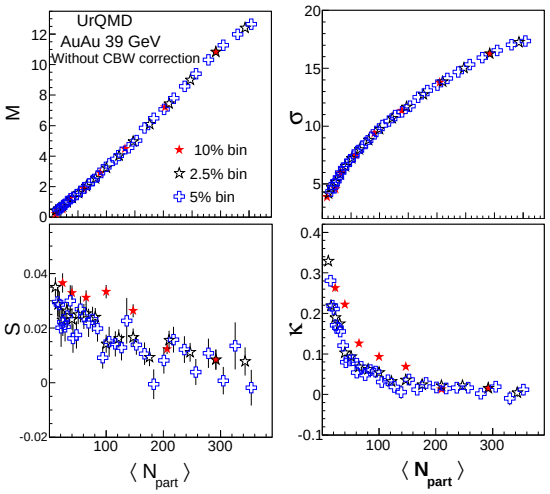

FIG. 2: Mean, standard deviation, skewness and kurtosis for Au-Au collisions at $\sqrt{s_{\rm NN}}$=39 GeV as a function centrality, expressed in terms of number of participating nucleons. These values are obtained for the net–charge distributions with centrality bins of 2.5%, 5% and 10%. In this figure, centrality bin width effect is not taken care of.

where the index i runs over each multiplicity bin, X_i represents various moments for the i-th bin, and n_i is the number of events in the i-th multiplicity bin. $\sum_i n_i = N$ is the total number of events in the centrality bin. Fig.3 shows corrected moments by using this method of centrality bin width correction. No centrality bin width dependence is observed in each of three different centrality classes. For the rest of the article, all the plots are made by using the centrality bin width correction of the moments and the statistical error of the above higher moments are estimated by the Delta theorem [22].

IV. EFFECT OF PARTICLE SPECIES ON HIGHER MOMENTS

Charged particles, produced in the collision, mostly comprise of π^+, π^-, K^+, K^-, p, and $\bar{p}$. All of these particle species contribute to the shape of the net–charge multiplicity distributions and hence to the moments of the distributions. To understand the contribution of different particles to the final net-charge higher moments, distributions for net-pion, net-kaon and net-proton are made separately, taking the particle identification at the event generator level. This has been studied for different centralities and different colliding energies. On the other hand, the leptonic contribution on the net–charge multiplicity distribution has very negligible effect [25].

In order to study the centrality dependence of the contribution from particle species for the moments of net–charge distributions, we have used the UrQMD event generator for Au-Au collisions at $\sqrt{s_{\rm NN}}$=39 GeV. All types of particles are selected in the same pseudo-rapidity ($|\eta| = 0.5$) window and same transverse momentum ranges ($0.2 < p_{\rm T} < 2.0$ GeV/c). Fig. 4 shows the M, σ, S and κ values of the net–charge, net–pion, net–proton and net–kaon distributions as a function of number of participant nucleus. We observe that except for net–pion, the mean of the other three distributions increase in going from peripheral to central collisions. The net–proton distributions dominate the mean of the net–charge distributions. For net–pions, the mean shifts towards negative value for central collisions. The width of the net–charge distribution is dominated by the net–pion distribution. Widths of the net–kaon and net–proton distributions are close together. The

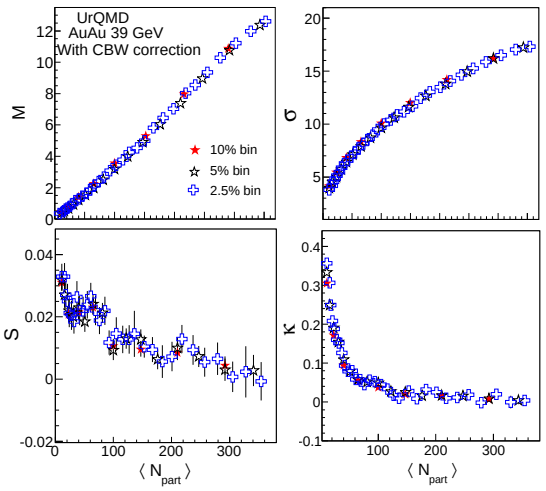

FIG. 3: Mean, standard deviation, skewness and kurtosis for Au-Au collisions at $\sqrt{s_{\rm NN}}$=39 GeV as a function centrality, after the bin width corrections are taken into account. The resulting moments of the distributions are close to each other for all three (2.5%, 5% and 10%) centrality bins.

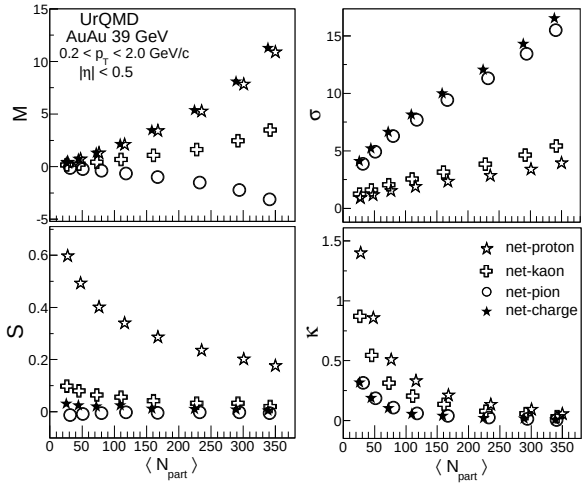

FIG. 4: Mean, standard deviation, skewness and kurtosis for Au-Au collisions at $\sqrt{s_{\rm NN}}$=39 GeV as a function centrality, expressed in terms of number of participating nucleons, for net–charge, net–pion, net–kaon and net-proton.

skewness for net–proton is obviously very different compared to other three sets, because of the difference between proton and anti-proton production in the collision. The skewness for net–charge is similar those of the net–pions. Similarly, the kurtosis values for net–charges are also close to those of net–pions. Thus different moments of the net–charge distributions are affected differently by net–pions, net–kaons and net–protons.

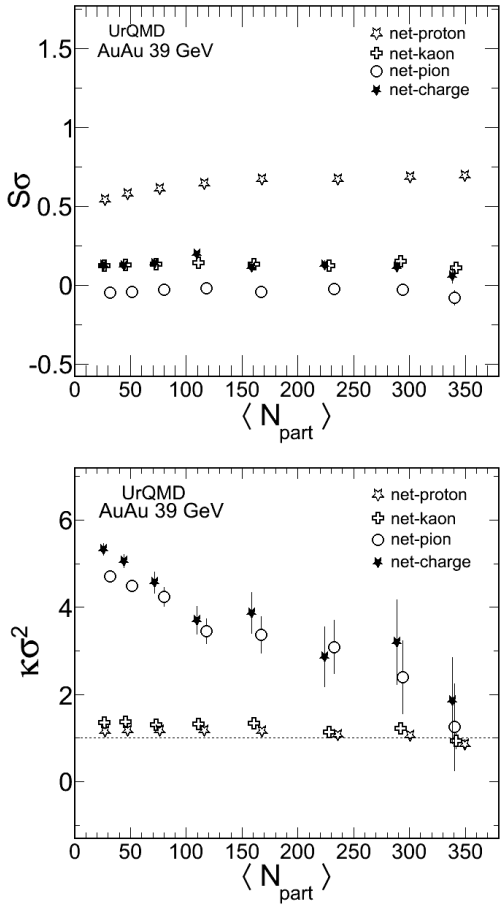

FIG. 5: Products of moments, $S\sigma$ (upper panel) and $\kappa\sigma^2$ (lower panel), plotted with respect to average number of participating nucleons, for net–charge, net–pion, net–kaon, and net–proton distributions.

In order to understand the contribution of different species on the product of moments, in Fig. 5 we show the products, $S\sigma$ and $\kappa\sigma^2$ as a function of centrality for different particle species. The $S\sigma$ values do not show any centrality dependence for net–charge or any other particle species. The $S\sigma$ values for net–charge are close to those of the net–pions, where are those of net–protons are much larger. The values of $\kappa\sigma^2$ for net–charges are dominated by those of the net–protons. A strong centrality dependence of the numbers is seen where $\kappa\sigma^2$ values for net–charge and net-protons decrease in going from peripheral to central collisions. For net–proton as well as for net–kaon, the $\kappa\sigma^2$ values are very close to unity with no centrality dependence.

It is known that the particle production mechanism for different particles depends on the center-of-mass energy of the collision. Thus as a function of

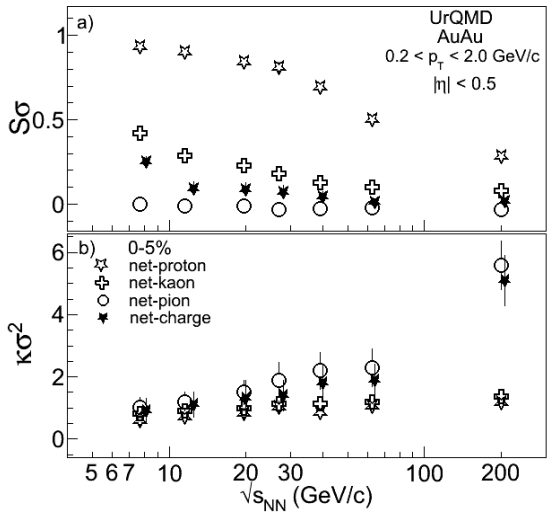

FIG. 6: Products of moments, $S\sigma$ (upper panel) and $\kappa\sigma^2$ (lower panel), plotted with respect to Au-Au collisions at different colliding energies. The moments are obtained from net–charge, net–pion, net–kaon, net–proton distributions.

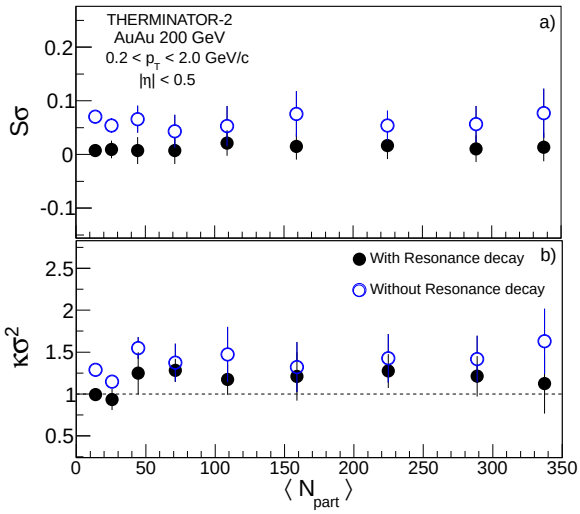

FIG. 7: The product of the moments, $S\sigma$ (upper panel) and $\kappa\sigma^2$ (lower panel), plotted with respect to average number of participating nucleons for two cases: with decay of all resonances and (ii) without resonance decays taken into account.

the beam energy, the distributions of the net–charge, net–pion, net–kaon and net–proton will be different, thus affecting the higher moments and their products. We have studied this in the UrQMD model, for top central (0-5%) collisions and as a function of beam energy, as shown in Fig. 6. For $S\sigma$, the energy dependence of net–proton is very prominent compared to net–kaon and net–charge, whereas no energy dependence is seen for net–pions. The $S\sigma$ values for net–charge are close to net–pions for most cases. For $\kappa\sigma^2$, no significant energy dependence is seen for net–proton or net-kaon. The energy dependence of net–charge is similar to that of the net-pions. Thus for both of the quantities shown in Fig. 6, energy dependence of net–charge is dominated by the net–pions.

V. RESONANCE EFFECTS ON HIGHER MOMENTS

In heavy-ion collisions, the abundance of resonance production may have its effect in net-charge higher moments in the finite pseudo-rapidity range. To study the effect of resonance decay on the net-charge higher moments analysis, we have used the thermal model like, THERMINATOR-2, for Au-Au collisions at $\sqrt{s_{\rm NN}}$ =200 GeV. In this model, we are able to track the particles in order to know its origin. In the process, we can study the effects of the resonances such as, Ξ, Δ^{++}, ρ, ϕ, and ω and their anti-particles. We have studied two cases: (i) with decay of the resonances, (ii) without resonance decays, where all the parent particles without any decay are considered. In Fig. 7, we present the results for $S\sigma$ and $\kappa\sigma^2$ of net–charge distributions, as a function of number of participating nucleons, with and without resonance decays. It is observed that for both the quantities, the behavior of the data with and without resonance decay do not change. The values in fact increases with resonance decays turned on.

VI. MODEL PREDICTIONS

Distribution of the number of charged particles as well as the net-charges are sensitive to particle production mechanisms. Different models use different methods for particle production. The HIJING model treats the heavy-ion collisions as a superposition of nucleon-nucleon collisions. It can be used to study the effect of jets and mini-jets on the produced particles. UrQMD, is a hadronic transport model including strings. It has been used successfully to describe stopping power and hadronic re-scattering. THERMINATOR-2 gives a good description for the thermal model of particle production. These models do not contain any physics which is sensitive to the critical point. Thus these models can provide a baseline study for the physics analysis specific to QCD critical point.

Net-charge distributions for the three models, HIJING, UrQMD and THERMINATOR-2 are con-

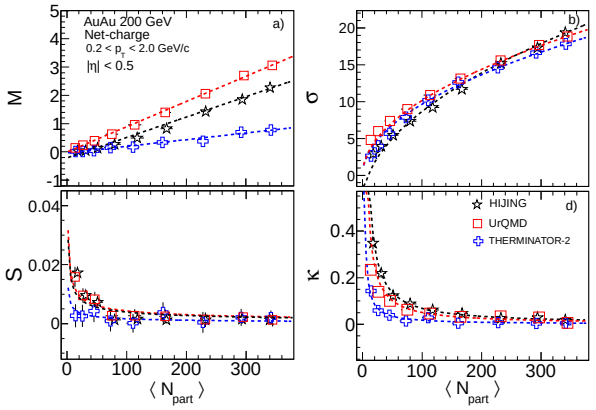

FIG. 8: The (a) mean, (b) standard deviation, (c) skewness, and (d) kurtosis, of net–charge distributions, plotted with respect to average number of participating nucleons for Au-Au collisions at $\sqrt{s_{\rm NN}}$ =200 GeV. The results from various models, such as HIJING, UrQMD and THERMINATOR-2 are plotted. Expectations from corresponding central limit theorem values are also superimposed in terms of dashed lines.

structed and analyzed to obtain the moments. Fig. 8 shows the M, σ, S and κ as a function of centrality for Au-Au collisions at $\sqrt{s_{\rm NN}}$=200 GeV for all the three models. The M and σ values increase in going from peripheral to central collisions for all the three models, whereas S and κ values decrease with increase in collision centrality. The mean value of net–charge is lower in THERMINATOR-2 as compared to HIJING and UrQMD models, but the standard deviation values are similar in all three cases. The centrality dependence of S for THERMINATOR-2 is also weaker compared to other two models.

The centrality evolution of the higher moments can be understood better by invoking the Central Limit Theorem (CLT) [23, 24], which gives the dependence of the moments on the number of participating nucleons. These are:

$$\begin{aligned} M &\propto N_{\rm part}, \\ \sigma &\propto \sqrt{N_{\rm part}}, \\ S &\propto \frac{1}{\sqrt{N_{\rm part}}}, \\ \text{and } \kappa &\propto \frac{1}{N_{\rm part}}. \end{aligned} \tag{3}$$

Here $N_{\rm part}$ is the average number of participating nucleons. The centrality evolution of the higher moments for all the three models follow the trend of the CLT in all the three models.

Connection to lattice QCD calculations can be made by carefully selecting the products of the moments, such as, M/σ^2, $S\sigma$ and $\kappa\sigma^2$. In Fig. 9 we show the M/σ^2, $S\sigma$ and $\kappa\sigma^2$ for 0-5% centrality

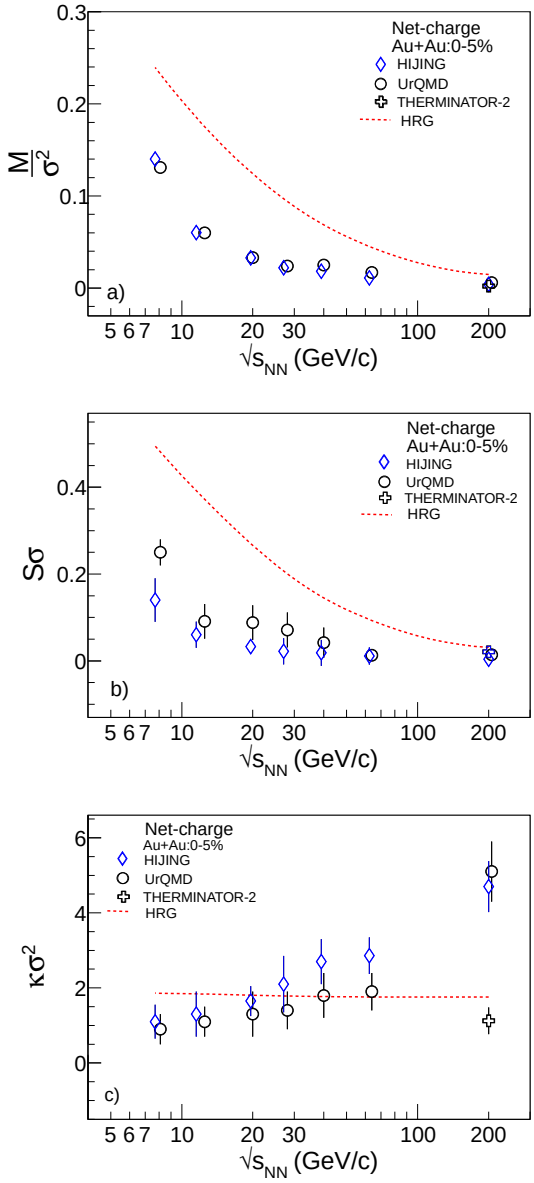

FIG. 9: The collision energy dependence of the (a) M/σ^2, (b) $S\sigma$ and $\kappa\sigma^2$ from net–charge distributions for top central (0-5%) collisions. The results are shown for HIJING, UrQMD, and THERMINATOR-2. The predictions from the Hadron Resonance Gas model for the net-charge are plotted in all cases.

for Au-Au collisions at $\sqrt{s_{NN}}$=7.7 to 200 GeV for the three models. In addition, prediction from the Hadron Resonance Gas (HRG) [26] model are superimposed on the plots. The M/σ^2, and $S\sigma$ values decrease with increase in colliding energy. All the three models are close to each other in these cases. The values of $\kappa\sigma^2$ remain consistent for all energies except at $\sqrt{s_{NN}}$ = 200 GeV for HIJING and UrQMD. The HRG prediction shows larger values than the

three models in M/σ^2, and $S\sigma$, but in $\kappa\sigma^2$, HRG model is very close to the three models except at 200 GeV. In the HRG and THERMINATOR-2, the thermal equilibrium consideration is taken into account for the particle production where as in the HIJING and UrQMD particles productions are taken place by Lund string model. This could be the reason for the discrepancy between thermal (HRG and THERMINATOR-2), and other models like HIJING and UrQMD.

VII. SUMMARY AND OUTLOOK

The study of higher moments of net–charge multiplicity distributions are proposed to be sensitive to the location of the critical point. In this manuscript, we have presented the higher moments of the net–charge distributions and their products for RHIC energies using HIJING, UrQMD and THERMINATOR-2 models. Net–charge distributions inherently contain contributions from net–pion, net–baryon (net–proton) and net–strangeness (net–kaon). To understand the effect of individual particles species on the net-charge distributions we have also studied net-pion, net-kaon and net-proton contributions. We observe that mean of the net–charge is dominated by net–protons whereas standard deviation, skewness and kurtosis are affected more by net-pion distributions. The resonance decay contributions to the net-charge distributions are studied by THERMINATOR-2 model. There is a small increase in $\kappa\sigma^2$ and $S\sigma$ of the net-charge distribution values due to the resonance decay in our acceptance. The various moments by the three models are compared for Au-Au collisions at $\sqrt{s_{\rm NN}}$=200 GeV and also compared with CLT expectations. Finally, all three model predictions are compared with expectation from HRG model for various colliding energies from $\sqrt{s_{NN}}$=7.7 to 200 GeV. Model calculations are compared for M/σ^2, $\kappa\sigma^2$ and $S\sigma$ for high (0-5%) central collisions. These models show regular behavior of the products of moments. These studies set the baseline understanding for the current experimental program at RHIC for locating the QCD critical point. The effects of global charge conservation, finite acceptance, and system size dependence on the net-charge distributions will be focused on a future study.

Acknowledgement

The authors would like to thank Bedangadas Mohanty, Xiaofeng Luo, Lizhu Chen, Prithwish Tribedy and Nu Xu for their valuable suggestions during the preparation of the manuscript.

[1] Y. Aoki et al., Nature **443** 675 (2006).
[2] S. Ejiri, Phys. Rev. **D 78**, 074507 (2008).
[3] E. S. Bowman and J. I. Kapusta, Phys. Rev. **D 79**, 015202 (2009).
[4] M. A. Stephanov, Prog. Theor. Phys. Suppl. **153** 139 (2004); Int. J. Mod. Phys. **A 20**, 4387 (2005).
[5] Z. Fodor et al., JHEP **0404**, 50 (2004).
[6] R. V. Gavai, S. Gupta, Phys. Rev. **D 78**, 114503 (2008).
[7] M. Cheng et al., Phys. Rev. **D 77**, 014511 (2008).
[8] M.A. Stephanov, Phys. Rev. Lett. **102** 032301 (2009).
[9] V. Skokov et al, arXiv:1108.3231 [hep-ph].
[10] Masakiyo Kitazawa et al., arXiv:1107.2755 [nucl-th].
[11] Adam Bzdak et al, arXiv:1203.4529 [nucl-ph].
[12] Adam Bzdak et al, arXiv:1206.4286 [nucl-th].
[13] A. Bazavov et al., arXiv:1208.1220 [hep-lat].
[14] Tapan K. Nayak (for the STAR collaboration) (QM2009) Nucl. Phys. **A 830** 555c (2009).
[15] M. M. Aggarwal et al. (STAR Collaboration), Phys. Rev. Lett. **105** 022302 (2011).
[16] M. M. Aggarwal et al., arXiv:1007.2613 [nucl-ex].
[17] J. Cleymans et al., Phys. Rev. **C 73**, 034905 (2006).
[18] Gyulassy M and Wang X N, 1994 Comput. Phys. Commun. 83 307; X. N. Wang and M. Gyulassy, Phys. Rev. **D 44**, 3501 (1991).
[19] S. A. Bass et al., Prog. Part. Nucl. Phys. **41** 255 (1998); M. Bleicher et al., J. Phys. G **25** 1859.
[20] Mikolaj Chojnacki, et al., arXiv:1102.0273; A. Kisiel et al., Comput. Phys. Commun. **174**, 669 (2006).
[21] Xiaofeng Luo (for the STAR Collaboration), arXiv:1106.2926.
[22] Xiaofeng Luo, J. Phys. G: Nucl. Part. Phys. **39**, 025008 (2012).
[23] X. F. Luo, B. Mohanty, H. G. Ritter and N. Xu, J. Phys. G **37**, 094061 (2010).
[24] Prithwish Tribedy et al., Phys. Rev. C **85** 024902 (2012).
[25] Nihar R. Sahoo (for the STAR Collaboration), arXiv:1101.5125 [nucl-ex].
[26] F. Karsch et al., Phys. Lett. B **695**, (2011).